GEOPHYSICS, VOL. 76, NO. 3 (MAY-JUNE 2011); P. R57–R67, 8 FIGS., 2 TABLES.
10.1190/1.3556120

Seismic characterization of thin beds containing patchy carbon dioxide-brine distributions: A study based on numerical simulations

J. Germán Rubino[1] and Danilo R. Velis[2]

ABSTRACT

We studied the seismic attenuation and velocity dispersion effects produced by wave-induced fluid flow in weakly consolidated sandstones containing patchy carbon dioxide (CO_2)-brine distributions. The analysis also focuses on the velocity pushdown because of the presence of this gas, as well as on the role of the wave-induced fluid flow (mesoscopic) effects on the amplitude variation with angle (AVA) seismic response of thin layers containing CO_2, such as those found at the Utsira Sand, Sleipner field, offshore Norway. We found that this loss mechanism may play a key role on conventional surface seismic data, suggesting that further data analysis may provide useful information on the characteristics of the fluid distributions in these environments. Numerical experiments let us observe that although mesoscopic effects can be very significant in this kind of media, the seismic response of a given isolated thin layer computed considering such effects is very similar to that of a homogeneous elastic thin layer with a compressional velocity equal to that of the original porous rock averaged in the effective data bandwidth. This suggests that the thin-bed prestack spectral inversion method published by the authors could be used to estimate representative compressional velocities and layer thicknesses in these environments. In effect, results using realistic synthetic prestack seismic data show that isolated CO_2-bearing thin beds can be characterized in terms of their thicknesses and representative compressional velocities. This information can be qualitatively related to CO_2 saturations and volumes; thus, the prestack spectral inversion method could find application in the monitoring of the evolution of CO_2 plumes at injection sites similar to that at the Sleipner field.

INTRODUCTION

Underground storage of carbon dioxide (CO_2) is an immediate option to reduce the amount of this greenhouse gas emitted to the atmosphere, and thus to mitigate climate change. Seismic methods constitute a very useful tool to monitor the injection of this gas because of the marked contrast between its acoustic properties and those of brine.

Since October 1996, an average of 1 million tons of CO_2 per year have been injected into the Utsira Sand at the Sleipner field, offshore Norway, with more than 11 million tons in the formation by 2010 (Chadwick et al., 2010). This formation is a weakly consolidated sandstone at depths between 800 m and 1100 m. Internally it contains thin intrareservoir shale layers, having typical thicknesses of 1–2 m and up to 6 m. The CO_2 is injected at a supercritical state near the bottom of the Utsira Sand, and it rises because of buoyancy effects until it reaches flow barriers such as the thin shale layers and the top seal shale. Beneath each intrareservoir shale, CO_2 accumulates following the structural relief and forms layers of up to a few meters thick (Arts et al., 2008). These thin layers can be identified in the seismic data as bright subhorizontal reflections, which are caused mainly by the high compressibility of the CO_2 as compared to that of the brine, and by constructive tuning effects of the top and bottom reflections at the CO_2 accumulations (Arts et al., 2004). The correct interpretation of the seismic responses of these structures is crucial to performing a proper monitoring of the injection process at the Sleipner field.

The major cause of seismic attenuation in reservoir rocks at seismic frequencies presumably is wave-induced fluid flow

Manuscript received by the Editor 24 September 2009; revised manuscript received 29 October 2010; published online 2 May 2011.
[1]Formerly Universidad Nacional de La Plata, Facultad de Ciencias Astronómicas y Geofísicas, La Plata, Argentina and CONICET, Argentina; presently University of Lausanne, Institute of Geophysics, Lausanne, Switzerland. E-mail: German.Rubino@unil.ch.
[2]Universidad Nacional de La Plata, Facultad de Ciencias Astronómicas y Geofísicas, La Plata, Argentina and CONICET, Argentina. E-mail: velis@fcaglp.unlp.edu.ar.

because of mesoscopic-scale heterogeneities, i.e., heterogeneities larger than the pore size but smaller than the predominant wavelengths (White, 1975; White et al., 1975; Pride et al., 2004; Carcione and Picotti, 2006). It long has been recognized that this loss mechanism is particularly important in the presence of rocks partially saturated with hydrocarbon gas and water because of the strong contrast between the physical properties of the pore fluids.

White (1975) and White et al. (1975) were the first to model this phenomenon, showing that this mechanism produces significant attenuation and velocity dispersion effects at seismic frequencies in partially saturated rocks. Since then, many authors have made important contributions to a better understanding of this subject, including a great variety of analytical solutions to model the seismic responses of rock samples containing heterogeneities of ideal geometries; see, for instance, Norris (1993), Johnson (2001), Pride and Berryman (2003). Other studies are based on numerical simulations of wave propagation, such as in Helle et al. (2003) and Rubino et al. (2007), among others. However, in the low-frequency range, these methodologies are computationally expensive or not feasible because the diffusion length associated with the fluid pressure equilibration is very small as compared with the seismic wavelengths.

Alternatively, Rubino et al. (2009) present an approach where numerical oscillatory compressibility and shear tests are applied to representative rock samples to obtain their equivalent complex undrained plane-wave and shear moduli. This upscaling procedure permits handling of complex geometries and also is computationally convenient, because the rock sample has to be much smaller than the wavelengths associated with the excitation frequencies.

As mentioned by Arts et al. (2004), the assumption of an homogeneous mixture of CO_2 and brine in the porous volume of the rocks with respect to the seismic wavelengths is likely to be fulfilled only approximately at the Sleipner field. In such a case, considering that the reservoir contains patches of CO_2 in a brine-saturated background, and taking into account the high porosity, high permeability, and low frame moduli of the Utsira Sand, together with the high compressibility of the CO_2, significant attenuation and velocity dispersion effects are expected to arise because of wave-induced fluid flow. These effects may play a key role in the observed seismic responses of these environments; thus, a better comprehension of this subject is needed. As far as we know, there are no published observations of attenuation for the Sleipner field, which would allow us to recognize these effects on the seismic data. Certainly, a deeper understanding of the mesoscopic mechanism in these environments would help to extract, from seismic data, useful information about the mesoscopic-scale characteristics of the CO_2-bearing layers, such as overall CO_2 saturation, nature of fluid distribution, and mean size of CO_2 patches, among others.

In this sense, questions such as whether the distribution of CO_2 within the Utsira Sand is patchy or homogeneous remain unanswered, for there is no clear evidence. It is an open question whether a patchy CO_2 saturation produces significant effects on conventional surface seismic data (Lumley, 2010). And in that case, assessing the possibility of being able to derive useful information about these environments from seismic data needs further investigation.

Different quantitative methods have been applied to the extensive data set of the Sleipner field, as clearly summarized by Chadwick et al. (2010). In particular, several authors have successfully applied elastic prestack or poststack inversion procedures to the real seismic data or to synthetic data representative of this injection site. For instance, Delépine et al. (2009) use a poststack stratigraphic inversion of the 1994 and 2006 data sets to obtain acoustic impedances for the Sleipner plume. In addition, Clochard et al. (2009) compare prestack and poststack inversion procedures, and verify that their prestack inversion methodology is feasible and useful in this environment.

Chadwick et al. (2010) describe other quantitative methods applied to the Sleipner data sets but focusing on the reservoir's topmost CO_2 accumulation. These methods include a topographic analysis that provides structurally derived thicknesses by assuming a velocity model for the overburden, and spectral decomposition algorithms, which provide temporal layer thicknesses and compressional velocities when constrained with independent true thickness estimates. Constrained amplitude variation with offset (AVO) analysis based on reflectivity modeling of subtuning layers with assumed petrophysical properties also has been used as a thickness classification tool. Clearly, given the complexity of these environments, the uncertainties associated with the various parameters involved, and the nonuniqueness of the modeling techniques, the quantitative determination of thin-layer thicknesses and velocities is a challenge and requires further investigation. As mentioned by Chadwick et al. (2010), the analysis and applications of these methods to real data from the Sleipner field are ongoing.

With these motivations, we first study the seismic attenuation and velocity dispersion effects that take place at a weakly consolidated sandstone, similar to the Utsira Sand, which contains patchy CO_2-brine distributions. We also analyze the role of this physical mechanism in the velocity pushdown effect, i.e., in the time shift observed in reflections within or below the CO_2 plume because of the presence of CO_2 in the pore space of the rock.

Next, we analyze the seismic response of CO_2-bearing thin beds such as those found at the Sleipner field, taking into account mesoscopic effects. With this aim, we follow Rubino and Velis (2009) to obtain the AVA response of CO_2-bearing thin beds embedded between two brine-saturated sandstones, taking into account the viscoelastic behavior of the CO_2 accumulations. To model the viscoelastic nature of the thin beds we employ the numerical method published by Rubino et al. (2009), which allows replacing a highly heterogeneous fluid-saturated porous rock by a viscoelastic solid with the same attenuation and velocity dispersion.

Finally, we use the prestack spectral inversion technique proposed by Rubino and Velis (2009) to evaluate the possibility of characterizing this type of thin beds. With the ultimate goal of estimating their thicknesses and CO_2 saturations from seismic data.

VISCOELASTIC BEHAVIOR OF ROCKS CONTAINING HETEROGENEOUS CO_2-BRINE DISTRIBUTIONS

As mentioned in the introduction, the propagation of seismic waves in rocks containing mesoscopic-scale heterogeneities in the fluid or frame properties may induce fluid flow. This physical process constitutes the dominant P-wave attenuation mechanism in reservoir rocks at seismic frequencies and can be understood as follows: When a compressional wave squeezes a heterogeneous

fluid-saturated porous material, the different regions of the medium — because of their distinct elastic properties — may undergo different pore-fluid pressures. This produces fluid flow and thus generates energy loss and velocity dispersion.

In our opinion, the role of these effects in seismic monitoring of CO_2 sequestration has not received as much attention as it deserves. As far as we know, there are no articles that study this topic in detail, with the remarkable exception of the paper by Carcione et al. (2006). These authors quantify these effects at the Utsira Sand, and observe that mesoscopic loss may be very significant at this geological formation. However, to obtain this information they employ the analytical White's model (White, 1975), which is valid strictly for spherical gas patches, and do not analyze the role of this physical mechanism in the velocity pushdown effects.

In this section we use the method presented by Rubino et al. (2009) to extract the viscoelastic behavior of rock samples containing highly heterogeneous quasifractal distributions of CO_2 and brine. Because we consider rock samples containing heterogeneities associated with pore-fluid distributions, shear tests produce unimportant mesoscopic effects. Thus, in the numerical examples shown in this work, we assume that the shear moduli of the rock samples are frequency independent, real, and equal to the shear moduli of their dry matrices.

Oscillatory compressibility test

Rubino et al. (2009) present a numerical upscaling procedure to obtain equivalent complex frequency-dependent plane-wave moduli for heterogeneous fluid-saturated porous rocks. In their method, a representative sample of the heterogeneous medium is subjected to a time-harmonic compression, and no tangential forces are applied on the boundaries of the sample. Following Rubino et al. (2009), the equivalent undrained complex plane-wave modulus $\bar{M}_c(\omega)$ can be expressed in terms of the amplitude of the time-harmonic compression and the (complex) oscillatory volume change, which is estimated solving Biot's equations of motion in the space-frequency domain under appropriate boundary conditions.

Then, the complex compressional velocity can be estimated using $V_{Pc}(\omega) = [\bar{M}_c(\omega)/\bar{\rho}_b]^{1/2}$, where $\bar{\rho}_b$ is the average bulk density of the rock sample. The equivalent compressional phase velocity $V_P(\omega)$ and (inverse) quality factor $Q_P(\omega)$ then are estimated using

$$V_P(\omega) = \left[\mathrm{Re}\left\{\frac{1}{V_{P_c}(\omega)}\right\}\right]^{-1}, \quad \frac{1}{Q_P(\omega)} = \frac{\mathrm{Im}\left\{V_{P_c}(\omega)^2\right\}}{\mathrm{Re}\left\{V_{P_c}(\omega)^2\right\}}. \tag{1}$$

We refer the reader to the work of Rubino et al. (2009) for the details of this numerical method.

Application to the Utsira Sand containing patchy CO_2-brine distributions

To analyze the amount of attenuation and velocity dispersion caused by heterogeneous fluid distributions, let us consider the Utsira Sand with a spatially variable CO_2-brine distribution in the form of irregular patches fully saturated with CO_2, and zones fully saturated with brine. We take into account neither mixing nor capillary forces, and we assume that the two fluids occupy different mesoscopic regions of the model. We consider neither chemical interaction between pore fluids and rock frame nor solubility effects.

We generate these (binary) heterogeneous distributions using stochastic fractal fields based on the so-called von Karman self-similar correlation functions, which are used widely in the statistical characterization of heterogeneities for different applications. Following Frankel and Clayton (1986), we consider a particular case for which the spectral density is given by

$$S_d(k_x, k_z) = S_0\left(1 + k^2a^2\right)^{-(H+E/2)}, \tag{2}$$

where $k = \sqrt{k_x^2 + k_z^2}$ is the radial wavenumber, a is the correlation length, H is a self-similarity coefficient $(0 < H < 1)$, S_0 is a normalization constant, and E is the Euclidean dimension. Equation 2 corresponds to a fractal process of dimension $D = E + 1 - H$ at scales smaller than a. In the experiments shown later, we take $E = 2$, $D = 2.5$, and different correlation lengths.

We first partition the computational domain (rock sample) into a finite number of square subdomains Ω_j, where j denotes cell number (we select 100×100 square cells in all cases) and assign to each Ω_j a pseudorandom number drawn from a uniform distribution. We then Fourier transform this field to the spatial wavenumber domain and filter its amplitude spectrum using equation 2. Then, we transform the result back to the spatial domain and obtain a microheterogeneous water saturation field $S_w^{(j)}$.

We obtain the final (binary) patchy field (i.e., the mesoscopic heterogeneities) by selecting a threshold S^* and setting each cell to zero-water saturation (i.e., 100% CO_2 saturation) or 100% water saturation according to whether $S_w^{(j)}$ is smaller or larger then S^*. In practice, we select S^* in such a way that an overall CO_2 saturation S_{CO_2} is obtained for each fractal field realization. Figure 1 shows some examples of the quasi-fractal fluid distributions considered in this work.

The next step is to compute the mesoscopic loss. For this purpose we need the rock frame and pore fluids' physical

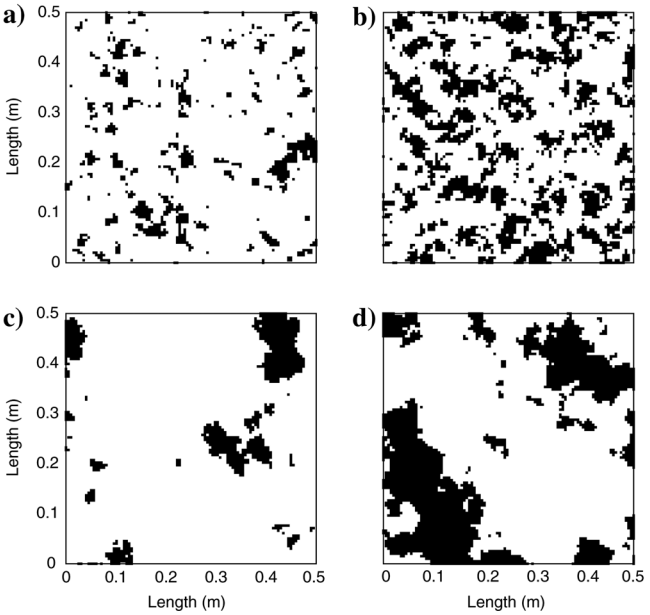

Figure 1. Examples of quasi-fractal distributions of CO_2 and brine in the Utsira Sand. (a) $a = 0.01$ m, $S_{CO_2} = 0.1$; (b) $a = 0.01$ m, $S_{CO_2} = 0.3$; (c) $a = 0.1$ m, $S_{CO_2} = 0.1$; (d) $a = 0.1$ m, $S_{CO_2} = 0.3$.

parameters. In this sense, we assume that the solid matrix of the rock sample is homogeneous and corresponds to the Utsira Sand, with properties given by Arts et al. (2004).

Following this work, we take a rock porosity $\phi = 0.37$, mineral bulk modulus $K_s = 36.9$ GPa, and solid grains density $\rho_s = 2.65$ gr/cm^3. Also, we consider a brine density $\rho_w = 1.09$ gr/cm^3 and bulk modulus $K_w = 2.3$ GPa. In addition we set, for full water saturation, $V_P = 2.05$ km/s and $V_S = 0.643$ km/s (Arts et al., 2004). Thus, using the inverse Gassmann's equation and the relation between shear velocity, bulk density and shear modulus, we obtain the rock frame bulk modulus $K_m = 2.68$ GPa, and the shear modulus $\mu_m = 0.857$ GPa. Also, water viscosity is taken to be $\eta_w = 1$ cP and rock permeability $\kappa = 1$ D.

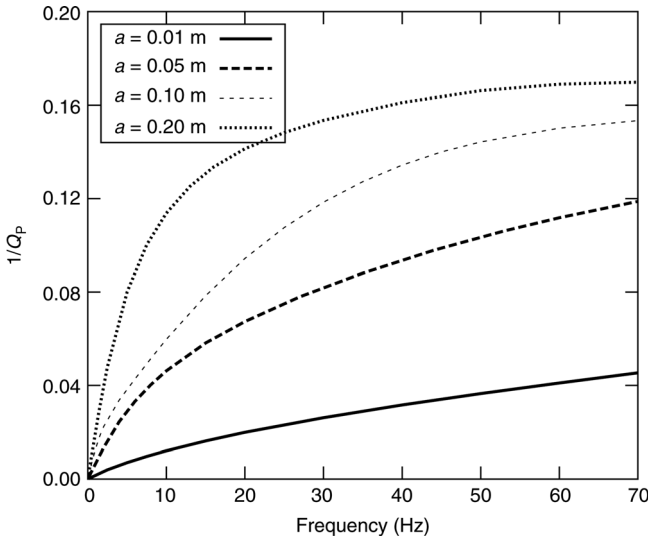

Figure 2. Equivalent inverse quality factor as a function of frequency, for rock samples containing an overall CO_2 saturation $S_{CO_2} = 0.1$ and different correlation lengths.

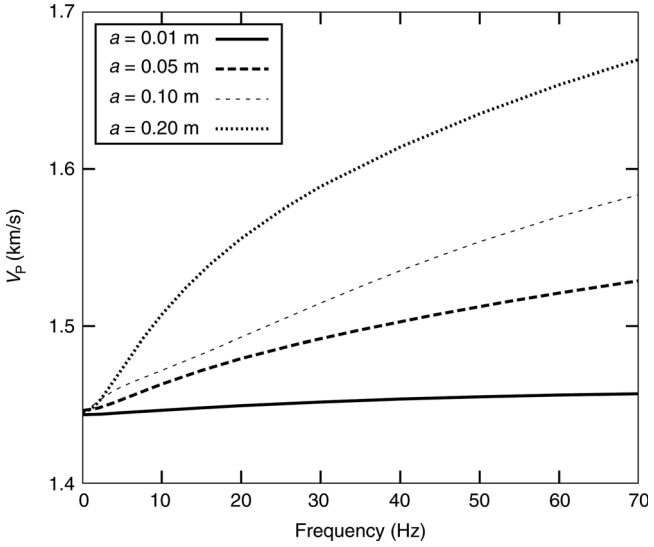

Figure 3. Equivalent compressional phase velocity as a function of frequency, for rock samples containing an overall CO_2 saturation $S_{CO_2} = 0.1$ and different correlation lengths.

We calculate the CO_2 density and bulk modulus employing the equation of state proposed by Duan et al. (1992), considering a temperature $T = 37°C$ and pressure $P = 10$ MPa, which are representative values for the reservoir under consideration. Thus, in the numerical experiments we set $\rho_{CO_2} = 0.693$ g/cm^3 and $K_{CO_2} = 0.0229$ GPa. In addition, we use Sutherland's formula to compute CO_2 viscosity as a function of temperature, obtaining $\eta_{CO_2} = 1.56 \times 10^{-4}$ P.

Figures 2 and 3 show, respectively, the equivalent compressional inverse quality factor and phase velocity as functions of frequency, for particular samples containing an overall CO_2 saturation $S_{CO_2} = 0.1$ and different correlation lengths. In all cases the samples are squares of side length $L = 0.5$ m, and we employ computational meshes of 100×100 equal square elements. It can be seen that the energy losses are very significant in the seismic frequency band, with quality factors below 10 in some cases, showing the importance of this loss mechanism in the behavior of the rock samples under consideration. We can observe significant velocity dispersion effects, mainly for correlation lengths above 0.1 m. On the other hand, the mesoscopic effects become less significant as patch size decreases.

These effects become less significant for CO_2 saturations higher or lower than about 0.1 (plot not shown for brevity). In the case of samples with $S_{CO_2} = 0.3$ and correlation lengths between 0.01 m and 0.2 m, for instance, although velocity dispersion increases with patch size, these relative changes do not exceed 5% in the frequency range considered. In addition, equivalent quality factor is below 10 only for the largest correlation lengths and for frequencies above 45 Hz.

Velocity dispersion effects on the velocity pushdown

The presence of CO_2 in the pore space of the rock produces a lowering of the compressional velocity, which may induce significant pushdown of reflections within or below the CO_2 plume. This effect is clearly seen in the time-lapse seismic data of the Sleipner field, and can be used to obtain additional information about the CO_2 distribution (Arts et al., 2004; Chadwick et al., 2005; Ghaderi and Landrø, 2009).

Because wave-induced fluid flow may produce significant velocity dispersion effects, we are interested in studying the role of this physical mechanism in the pushdown, an analysis not formally performed previously.

With this objective, and taking into account that we are dealing with rocks having local properties drawn from certain probability distribution function, we apply a Monte Carlo analysis similar to that suggested by Rubino et al. (2009) to extract the statistical characteristics of the pushdown as functions of overall CO_2 saturation, correlation length, and frequency. We consider different saturation values, frequencies, and correlation lengths, and for each set of parameters we generate a large number of realizations N_r. Next, for each realization we obtain the equivalent compressional phase velocity, V_P^i, $i = 1, \ldots, N_r$, and calculate the pushdown factor (i.e., the time delay corresponding to a 1-m-thick layer) using (Chadwick et al., 2005)

$$2\left(\frac{1}{V_P^i} - \frac{1}{V_P}\right), \tag{3}$$

where V_P is the compressional velocity of water-saturated rock ($V_P = 2.05$ km/s). Then, we obtain the mean and standard deviations of the pushdown factor, which represent the statistical behavior of the samples under consideration. To ensure convergence of the Monte Carlo approach, we consider a criterion similar to that shown by Rubino et al. (2009), i.e., for each set of parameters we check that after N_r realizations the variance of the pushdown factor, as a function of the number of realizations, stabilizes at a constant value.

Figure 4 shows the mean pushdown factor plus-minus one standard deviation for three correlation lengths and $S_{CO_2} = 0.1$ (dotted and dashed lines), as functions of frequency. In each case we set $N_r = 70$ and check that the convergence criterion is satisfied. We can observe that the pushdown strongly depends on frequency, mainly for large correlation lengths. For instance, for $a = 0.2$ m there is a decrease of almost 30% between 10 and 50 Hz. It is interesting that the lower the frequency the lower the uncertainty. This is because for very large wavelengths the medium is *seen* as homogeneous, independently of the realization. As frequency increases, the wavelengths start to see differences among realizations, with the consequent increase in standard deviations.

We analyzed the statistical behavior of samples containing $S_{CO_2} = 0.9$ and for the same three correlation lengths used in the previous experiments. However, because for such high CO_2 saturation values velocity dispersion effects are negligible, there are no differences among the responses obtained using the different correlation lengths (Figure 4, solid line; note that the three curves coincide). In addition, the pushdown does not depend on the frequency in these cases and the uncertainty is negligible.

This analysis shows that the velocity dispersion effects may play a key role in the velocity pushdown, mainly when CO_2 concentrations are low; thus, seismic data at the Sleipner field may contain important additional information that may be used to improve the knowledge of this reservoir.

Mean equivalent compressional velocity and attenuation

The fact that seismic data contain errors of different nature and magnitude, and that their energy is concentrated within a relatively narrow frequency range, suggests that they will at most provide information about a single-phase velocity and a single quality factor that are representative of that narrow bandwidth.

For this reason, and from a practical point of view, we average the compressional phase velocities and quality factors in a given effective data bandwidth for a large number of rock samples, and plot them as functions of overall saturation and correlation length.

Accordingly, Figure 5a shows the equivalent compressional phase velocity, as a function of CO_2 saturation and for various correlation lengths, averaged in the frequency range 10–60 Hz for a large number of realizations. This plot also includes the low-frequency limit velocity (solid line), which we compute taking into account that at sufficiently low frequencies the fluid pressure is uniform (isostress state); thus an effective fluid with bulk modulus given by Wood's law (Carcione and Picotti, 2006) can be used. Figure 5a shows that mean compressional phase velocities are higher than the low-frequency limit values. These differences are because of velocity dispersion effects and are more significant for large correlation lengths and S_{CO_2} near 0.1. On the contrary, for the correlation lengths considered in this work, we can observe that for CO_2 saturations above 0.3–0.4 or near zero, or for very small patch sizes, average velocities are very close to the low-frequency limit.

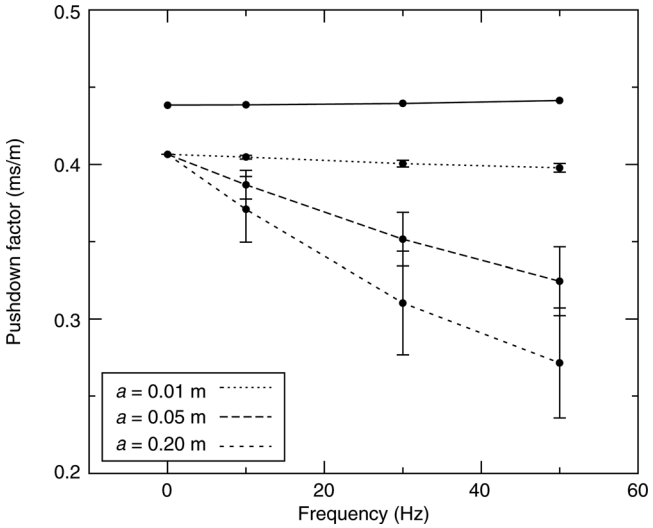

Figure 4. Mean pushdown factor (dots) plus-minus one standard deviation as a function of frequency, for three different correlation lengths. Dotted and dashed lines correspond to $S_{CO_2} = 0.1$, while the solid line corresponds to $S_{CO_2} = 0.9$.

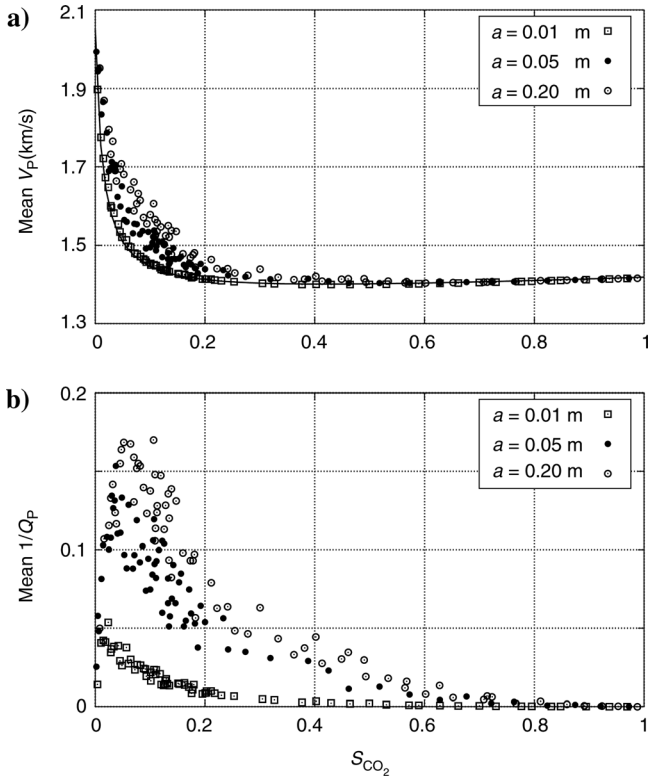

Figure 5. (a) Mean equivalent compressional phase velocity and (b) inverse quality factor as functions of CO_2 saturation, for different realizations and correlation lengths.

Equivalent compressional quality factors also were averaged within the same bandwidth and for the same set of realizations (Figure 5b). These data show that very important attenuation levels take place in these experiments, and become more significant as the characteristic size of the patches increases. The average quality factors take values below 10 for S_{CO_2} near 0.08 and correlation lengths above 0.05 m. This behavior corresponds to that observed in Figure 5a, because higher attenuation levels usually are associated with higher levels of velocity dispersion. For CO_2 saturations near zero or above 0.6, approximately, average quality factors take values above 100. In the particular case of very small CO_2 patches, this parameter is above 100 for saturations above 0.2, approximately.

This analysis, which as far as we know is the broadest and most complete of its kind, shows that seismic data associated with rocks with patchy distributions such as those considered in this work are expected to carry information that may help to provide a broad insight about CO_2 saturation values. In addition, these results show that for the patch sizes considered in this work, mesoscopic effects are more significant for CO_2 saturations near 0.1 and large correlation lengths. If CO_2 saturation is higher than 0.6 or close to zero, attenuation and velocity dispersion effects can be disregarded irrespective of the patch size. Therefore, in these cases, CO_2-bearing rocks behave like an elastic solid with a compressional velocity given by that of the low-frequency limit. For very small patch sizes, this approximation is valid for S_{CO_2} higher than about 0.2.

SEISMIC RESPONSE OF A CO_2-BEARING THIN BED

As mentioned in the introduction, in the Utsira Sand, CO_2 accumulates beneath thin intrareservoir shales, forming thin CO_2-bearing layers that can be identified in the seismic data as bright subhorizontal reflections. The results shown in the previous section demonstrate that seismic attenuation and velocity dispersion effects associated with wave-induced fluid flow may be very significant in these media; thus, they may play a key role in the observed seismic responses.

In this section we analyze the seismic responses of thin layers containing heterogeneous distributions of CO_2 and brine in the AVA domain. We use a method similar to that presented by Rubino and Velis (2009) to obtain the AVA response of a thin bed embedded between two homogeneous half-spaces but, in this case, we include the viscoelastic behavior of the CO_2-bearing layer. It is important to remark that in the modeling we neglect the ultra-thin shale layers (1 to 2 m thick) typically found at the Utsira Sand because the contrast between the acoustic impedance of the water-saturated shale layers and that of the water-saturated sandstone is very low.

METHOD

Let us consider a horizontal layer embedded between two elastic homogeneous half-spaces. Taking into account a unit amplitude harmonic compressional plane wave of frequency $\omega = 2\pi f$ arriving at the thin bed with an incidence angle θ, we find relationships between the scalar and vector potentials associated with the compressional and shear wavefields traveling upward and downward in the different media of the model. After solving for the potential amplitude associated with the reflected compressional wave and multiplying it by the source amplitude spectrum, we obtain the spectra of the prestack data for different incidence angles. We refer the reader to the work of Rubino and Velis (2009) for the details of the calculations.

To take into account the viscoelastic nature of the thin layer, the wavenumber associated with the compressional wave and the Lamé constant λ_c should be taken as complex and frequency dependent. To compute them, we consider a compressional plane wave propagating through such a viscoelastic medium, and relate the inverse quality factor and phase velocity with the modulus of the wave vector, k^P, in the form

$$V_P(\omega) = \frac{\omega}{\mathrm{Re}(k^P)}, \tag{4}$$

$$\frac{1}{Q_P(\omega)} = -2\frac{\mathrm{Im}(k^P)}{\mathrm{Re}(k^P)}. \tag{5}$$

Then, we can express the modulus of the wave vector as

$$k^P = \frac{\omega}{V_P(\omega)}\left[1 - \frac{i}{2Q_P(\omega)}\right]. \tag{6}$$

In addition, the equivalent complex undrained plane-wave modulus can be written as $\overline{M}_c(\omega) = \lambda_c + 2\mu_m$, where μ_m is the shear modulus of the saturated rock. Thus, λ_c is complex and frequency dependent, and can be expressed as

$$\lambda_c = \overline{M}_c(\omega) - 2\mu_m. \tag{7}$$

In summary, for each frequency we apply the oscillatory compressibility test to obtain the equivalent phase velocity, quality factor and complex plane-wave modulus. Next, using equations 6 and 7 we compute k^P and λ_c.

Numerical experiments: Elastic versus viscoelastic models

With the aim of analyzing the effects of the mesoscopic loss on the seismic behavior of CO_2-bearing thin beds such as those found at the Utsira Sand, we apply the recently presented method to obtain the seismic responses of these structures considering different thicknesses, incidence angles, and CO_2 saturations. In all the examples we use a 30-Hz Ricker wavelet and a correlation length $a = 0.1$ m.

Figure 6 shows some particular realizations of the seismic responses of layers with thicknesses $h = 5$ and $h = 10$ m, containing two different CO_2 saturations, for two incidence angles (solid lines). In all cases there is an increase in the reflectivity with the angle of incidence and with CO_2 saturation. The last point is explained by the fact that the bed mean-phase velocity is lower for $S_{CO_2} = 0.3$ than for $S_{CO_2} = 0.1$; thus the contrast between the acoustic impedance of the thin bed and that of the water-saturated sandstone is more significant. In addition, the reflectivity is stronger in the case $h = 10$ m as compared with $h = 5$ m, as a consequence of the tuning effects for the considered wavelet.

Figure 6 shows the seismic responses obtained after replacing the (viscoelastic) thin layer by an elastic bed with the same shear velocity and bulk density, but with a compressional velocity

similar to that of the heterogeneous CO_2-bearing bed averaged in the effective data bandwidth (dashed lines). As expected, the discrepancies between the elastic and viscoelastic models are more significant for $S_{CO_2} = 0.1$, because mesoscopic effects are particularly important for this saturation value. However, it is interesting that although wave-induced fluid flow effects are very significant in these media, the discrepancies are negligible.

To understand this we have to take into account that the differences between the seismic responses are associated with energy losses within the bed and with velocity dispersion effects on the acoustic impedance contrasts between the layer and the upper and lower half-spaces. Energy loss effects are not significant because the layer is very thin as compared with the predominant wavelengths of the seismic waves. In addition, because the elastic model considers the mean-phase velocity computed within the frequency range in which the data contain most of the energy, the differences because of velocity dispersion effects are minimized. It is important to remark that if we consider a model with many thin beds, we would have a cumulative effect; thus, attenuation effects would play an important role. However, in this work we assume that the seismic response of the target thin layer does not interfere with that of other layers, and transmission and absorption losses associated with the overburden are included in the source spectrum through an appropriate well calibration at the target interval.

PRESTACK SPECTRAL INVERSION OF SEISMIC DATA FOR THE CHARACTERIZATION OF CO_2-BEARING THIN BEDS

As we mentioned in previous sections, the patchy nature of the CO_2 accumulations adds complexity to the modeling of the seismic response of this kind of structures. If we wish to extract useful information from the seismic data to fully characterize CO_2-bearing layers below tuning thickness, we must assume a simplified model. In this sense, the similarities between the elastic and viscoelastic seismic responses shown in Figure 6 and analyzed in the previous section suggest that the prestack spectral inversion method proposed by Rubino and Velis (2009) and originally devised to deal with elastic thin beds could be used to study thin beds containing patchy CO_2-brine distributions. This inversion procedure carries out the estimation of the thin-bed parameters in the frequency (amplitude spectrum) domain using simulated annealing (SA) and considering AVA data.

In contrast to using zero-offset data, the use of AVA data contributes to increasing the robustness of this inverse problem under noisy conditions, as well as to reduce significantly its inherent nonuniqueness. To further reduce the nonuniqueness, this method permits imposition of appropriate bounding constraints to the parameters of the media above and below the thin bed, which need not be known accurately. In addition, the use of simulated annealing to minimize the cost function permits us to avoid local minima and poor convergence, which are usual difficulties arising in this kind of geophysical problem.

With this purpose, in this section we invert the seismic response of thin beds in the prestack spectral (amplitude) domain, assuming an elastic layer embedded between two homogeneous half-spaces. We generate realistic data for thin beds similar to those found at the Utsira Sand, taking into account their viscoelastic natures because of mesoscopic effects. We consider several CO_2 saturations, correlation lengths and bed thicknesses. Because the rock properties are sampled randomly from a certain probability distribution function, we generate a large number of realizations and invert the resulting data in each case.

Following the procedure proposed by Rubino and Velis (2009), let $A(f,\theta)$ and $\hat{A}(f,\theta)$ be the amplitude spectra of the observed and calculated prestack data, respectively. Then, let J be a function that measures the discrepancies between $A(f,\theta)$ and $\hat{A}(f,\theta)$. Here, J is a 10-dimensional cost function that depends on the elastic properties and densities of the top and bottom half-spaces, and on the thickness, density, and elastic properties of the thin bed. Notice that although the simulated data assume that the top and bottom half-spaces have the same elastic properties, in the actual inversion these parameters are allowed to vary independently. Cost function J is given by

$$J = \frac{1}{NM}\sum_{i=1}^{N}\sum_{j=1}^{M} w_i\left[A(f_j,\theta_i) - \hat{A}(f_j,\theta_i)\right]^2, \qquad (8)$$

where N is the number of incidence angles, M is the number of frequencies, and w_i are weights. The minimization of J with respect to the model parameters represents a highly nonlinear inverse problem that can be solved conveniently using a hybrid optimization scheme that involves simulated annealing and a linearizing approach, as outlined by Rubino and Velis (2009). Note that in the actual computations, $A(f,\theta)$ represents the seismic

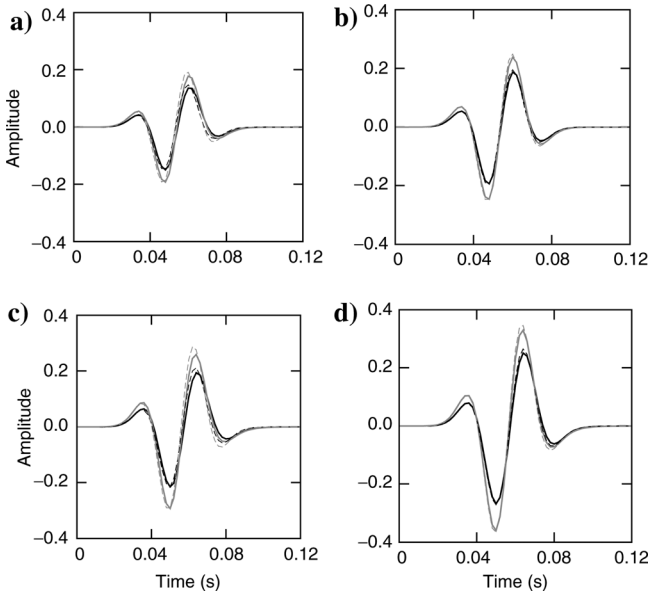

Figure 6. (a, b) Seismic responses for a 5-m, and (c, d) 10-m thick bed, for $S_{CO_2} = 0.1$ (a, c), and $S_{CO_2} = 0.3$ (b, d). Black lines correspond to an incidence angle $\theta = 0°$, while gray lines correspond to $\theta = 40°$. Solid lines represent the responses obtained taking into account the viscoelastic nature of the thin bed, while dashed lines are obtained by replacing the thin layer by an elastic bed with a mean compressional velocity.

response of the CO_2-bearing thin bed taking into account its viscoelastic properties, as discussed in previous sections. Contrarily, $\hat{A}(f,\theta)$ is calculated by assuming an elastic bed.

Results and Discussion

In practice, we obtain $A(f,\theta)$ from the observed data after isolating the seismic response of the CO_2-bearing thin bed in the time-angle domain using an angle-dependent time window. This process is illustrated in Figure 7, where we show a typical angle gather used in the inversion together with the angle-dependent time window (we use a Hamming window to avoid truncation effects). Then, we obtain $A(f,\theta)$ by applying the Fourier transform to the windowed data and taking the modulus.

The data used in the following numerical tests were obtained as follows. First, we calculated the AVA response of the viscoelastic thin-bed model in the frequency domain for incidence angles in the range $0°-40°$ and considering a 30 Hz-Ricker wavelet. Then, after applying the inverse Fourier transform, and

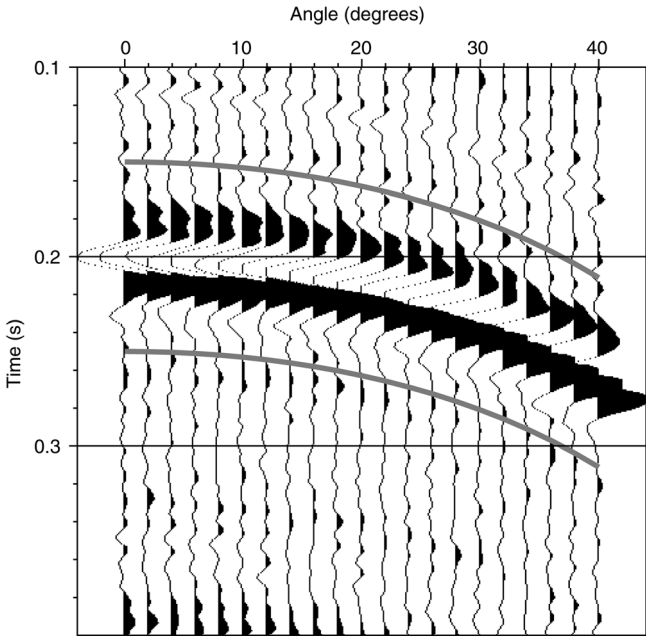

Figure 7. Typical prestack data used in the inversion. The hyperbolic gray lines show the angle-dependent window used to isolate the assumed CO_2-bearing thin bed seismic response. In this particular case, $h = 10$ m, $S_{CO_2} = 0.1$, and $a = 0.1$ m.

Table 1. Search ranges used in the inversion.[a]

Layer	V_P (km/s)	V_S (km/s)	ρ (g/cm^3)
Top half-space	2.0–2.2	0.6–0.7	2.0–2.2
CO_2-bearing thin bed	1.3–2.2	0.5–0.7	1.9–2.1
Bottom half-space	2.0–2.2	0.6–0.7	2.0–2.2

[a]The thickness of the CO_2-bearing thin bed is allowed to vary in the range 2–25 m. For the two half-spaces, we assume that their true properties are $V_P = 2.05$ km/s, $V_S = 0.643$ km/s, and $\rho = 2.073$ g/cm^3.

to simulate realistic data, we added two types of noise: additive and convolutional. The additive noise consisted of the summation of pseudorandom numbers drawn from a Gaussian distribution. For convenience, random noise was filtered previously with a 5 to 100 Hz passband filter. The convolutional noise was added, on the other hand, with the aim of simulating the effects of small reflectors that may be present in the data. These reflectors can be associated with the presence of the underburdens and overburdens. In this sense, we chose an arbitrary set of well-log data to construct an angle-dependent reflectivity using approximate Zoeppritz formula. Subsequently, we convolved this reflectivity with the source wavelet and added the result to the data. Finally, we applied a constant hyperbolic moveout to each trace. Figure 7 shows a typical gather constructed this way and used in the tests that follow.

During the inversion process, we consider bounding constraints in all the model parameters to guarantee physically reasonable models and to allow for the incorporation of a priori information. This is accomplished by selecting narrow search ranges for those parameters whose values are known approximately from other means (e.g., well-log data). On the other hand, we set wide search ranges for those parameters where this extra information is not available.

In a practical context, for the inversion of the seismic responses of the CO_2-bearing thin beds we assume that densities and velocities of the two half-spaces are known within a tolerance error of about $\pm 5\%$, but density, thickness, and velocities of the thin bed are allowed to attain any value within much wider search ranges (see Table 1). As noticed, the search ranges for the S-wave velocity and the density of the CO_2-bearing layer are in fact relatively narrow, because these quantities do not vary significantly for different CO_2 saturations, and reasonable estimates are available based on previous works (e.g., Arts et al., 2004).

To analyze the performance of the inversion procedure in different scenarios, we carried out a large number of inversions for different CO_2 saturations, correlation lengths and thicknesses. For simulating the seismic response of the thin layers we selected a Ricker wavelet, whose tuning thickness can be estimated using the expression $\sqrt{6}/(2\pi f_0)$, where f_0 is the dominant frequency (Chung and Lawton, 1995). In the case of a 30-Hz Ricker wavelet, the tuning thickness is about 13 ms, which turns out to be about 10 m for CO_2-bearing beds such as those found at the Utsira Sand. In the numerical examples that follow, we used thicknesses of 4, 7, and 10 m. In all cases we added noise to the data with a signal-to-noise ratio (S/N) of about 10 (by amplitude) and chose the 10–60 Hz band for the computation of the cost function J (we set all weights equal to one). As a result, the effective S/N ratio in the 10–60 Hz band is about 23 dB.

In addition, for each realization we averaged the results of 100 inversions, where each inversion involved the same data but different SA seeds. We used this strategy because of the difficulties associated with the minimization of the cost function J, which often does not show a very clear global minimum. Consequently, slightly different sets of model parameters led to excellent data fits. Nevertheless, because the variability of the compressional velocity and thickness estimates was small, we assumed that these averaged values correspond to the optimum solution within the global minimum region of the 10-dimensional model space.

Figure 8a shows, as a function of CO_2 saturation, the estimated compressional velocity for a 10-m-thick CO_2-bearing layer considering three different correlation lengths ($a = 0.01$, 0.05, and 0.2 m). In particular, for each of the correlation lengths, we took into account 70 realizations associated with different CO_2 saturations randomly distributed in the range 0–1. We can observe that for very low CO_2 saturations, there is a rapid increase in the compressional velocity for decreasing saturations. On the other hand, for saturations above 0.2, no significant velocity changes are appreciated.

Because mesoscopic effects are much more significant for CO_2 saturations about 0.1, the elastic model used to fit the actual viscoelastic response becomes less appropriate in these cases. In addition, at these saturation values the compressional velocity is very sensitive to the geometry of the CO_2 patches. As a consequence, it turns out that the dispersion of the inverted velocity is larger at these saturation levels, as can be observed in Figure 8a. Contrarily, when CO_2 saturations are relatively high (say above 0.2), the fit is much more accurate and the compressional velocity is less sensitive to the pore fluids distribution; thus, the variability of the inverted velocity is smaller.

It is interesting to see that the uncertainty of the inverted velocity is significantly lower for very small correlation lengths (e.g., squares in Figure 8). This can be explained by noting that for the frequencies considered in this work, the patches are very small and the wavelengths do not *see* differences among realizations.

Figure 8b and 8c show the results obtained for CO_2-bearing layers of thicknesses 7 m and 4 m, respectively. We can observe that the results obtained in these cases show similar behaviors to those found for a 10-m-thick bed.

Figure 8 can be compared with Figure 5a, where we plotted, for several CO_2 saturations and correlation lengths, the compressional velocity associated with the Utsira Sand containing patchy CO_2-brine distributions, averaged in the bandwidth 10–60 Hz. The similarities between the plots suggest that, although the inverted velocities shown in Figure 8 are not expected to attain the same numerical values as those in Figure 5a, their behaviors with respect to S_{CO_2} are comparable. The inverted velocities are, in fact, model parameters associated with a (simple) elastic thin-bed model that produces a seismic response similar to that of the viscoelastic model at different saturation levels. This fit is valid, at least, within the frequency range where the observed seismic energy is concentrated, which coincides with the bandwidth selected for the inversion. Thus, considering that the mean velocities shown in Figure 5a exhibit a clear relationship with CO_2 saturations, we believe that the inverted velocities shown in Figure 8 can be used as a petrophysical attribute to characterize CO_2-bearing thin beds in terms of saturations.

In effect, take Figure 8a as a reference. The gray bars show the mean (binned) inverted compressional velocity plus-minus one standard deviation, as a function of CO_2 saturation (bin size 0.1). These bars can be used as a guide to associate inverted velocities with S_{CO_2}. It is clear from the graph that in general, relatively high compressional velocities are associated with low (below 0.2) CO_2 saturations. On the other hand, velocities lower than about 1.45 km/s are indicative of S_{CO_2} higher than about 0.2. It is not possible to make any distinction among saturations above 0.2 because the inverted velocities do not show any significant change for these saturation values. On the contrary, the analysis shows that the inverted velocities may help discriminate qualitatively among saturations below 0.2, but in a broad sense, because the correlation length is not known.

On the other hand, the uncertainty of the inverted velocities increases, as expected, for thicknesses below tuning (see Figure 8b and 8c), especially for large correlation lengths. Here, the uncertainty is viewed as the dispersion of the inverted velocity and is represented in the graphs by the gray bars. As in the previous case, for these layer thicknesses high inverted velocities are indicative of low saturation values, while low velocities are associated with saturations above 0.2.

It is important to remark that should the patchy distribution be of known correlation length, the dispersion of the inverted

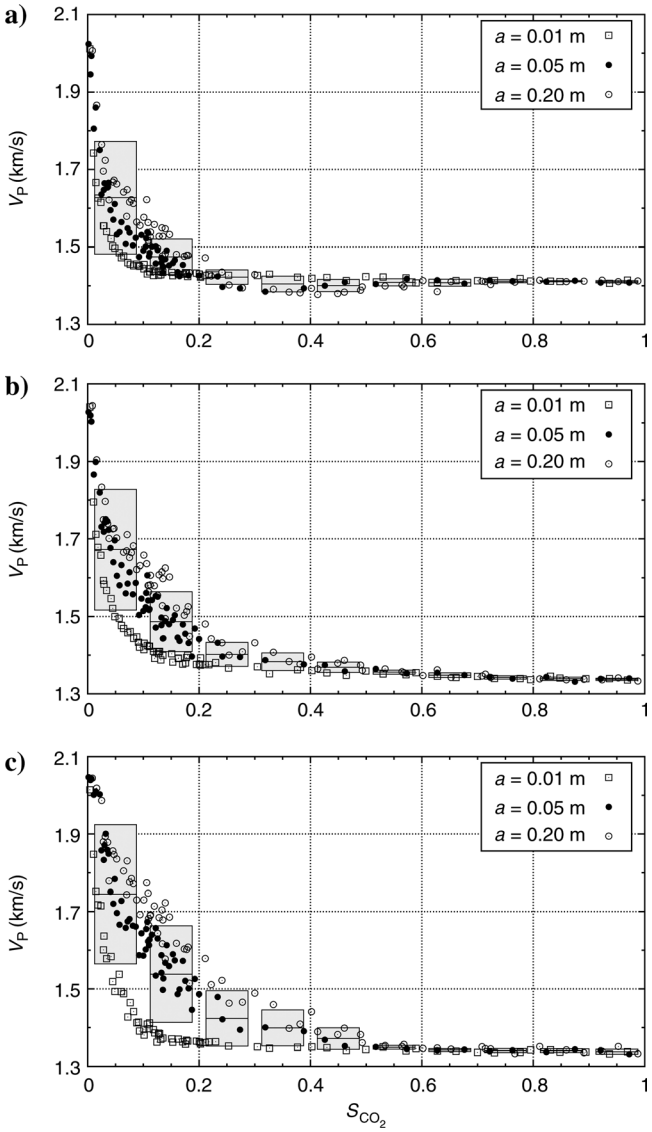

Figure 8. Estimated compressional velocity as a function of CO_2 saturation for a layer thickness of (a) $h = 10$ m, (b) $h = 7$ m, and (c) $h = 4$ m. In each case we consider three correlation lengths (denoted in the figure's legend) and a large number of realizations. For each realization, the associated dot represents the average of 100 different inversions performed on the corresponding synthetic data. Gray bars show the mean (binned) velocity plus-minus one standard deviation (bin size 0.1).

velocity in Figure 8 would be much smaller; thus it would be possible to draw more certain conclusions about CO_2 saturations. Naturally, the fact that in general the correlation length is not known limits the potentiality of these results, especially for very thin beds. For this reason, we believe that the inverted velocities can be used only as a guide to infer broad information to characterize qualitatively CO_2-bearing thin beds.

In addition to the thin-bed compressional velocity, the other parameter of interest is layer thickness. Table 2 shows the mean and standard deviation of the inverted thicknesses for three different CO_2 saturation ranges, taking into account the values obtained for the three correlation lengths. As expected, the larger the thickness and CO_2 saturation, the smaller the uncertainty. For $h = 10$ m, the accuracy of the inversion is very high, even for low-saturation values. As the layer thickness decreases, the accuracy becomes smaller; however, even in the case of a 4-m-thick bed the estimates are reasonable and may be very useful to improve knowledge of the distribution of the injected CO_2 in the formation.

It is important to emphasize that the thin-bed analysis and results presented in this work are limited to models consisting of a single viscoelastic layer embedded between two elastic half-spaces. Multilayer and other complex models are beyond the scope of this work. Hence, a key assumption is that the seismic response of an individual CO_2-bearing thin layer can be isolated from the seismic data using appropriate tapering windows, and that these data have been preprocessed properly for true amplitude. Transmission and absorption losses associated with the overburden are assumed to be included in the source spectrum, information that can be obtained through proper well calibration at the target interval. These assumptions also were utilized by Ghaderi and Landrø (2009) for estimating thickness and velocity changes using prestack time-lapse seismic data in the Sleipner field. On the other hand, typical problems related to phase changes with offset and NMO stretch effects are not an issue for the spectral inversion method, for it relies on amplitude spectra only.

Finally, it is worth mentioning that the results suggest that the proposed spectral inversion method may be used as a qualitative interpretation tool to characterize CO_2-bearing thin beds in a 2D or 3D framework. In this sense, it would be possible to obtain useful information about how the layer develops areally and what the CO_2 plume extension is within that unit. Presumably, at points far away from the injection point the CO_2 saturations are low; thus the extension of CO_2 plume could be delimited by detecting those regions where the inverted compressional velocity is relatively high. On the other hand, because zones with relatively low velocities are indicative of high CO_2 saturations, the procedure could be used to monitor in time and in space the extent of the CO_2 distribution, as well as how it migrates to the nearby zones around the injection point.

Table 2. Mean and standard deviation of the inverted thickness for different CO_2 saturation ranges.[a]

Actual thickness	$S_{CO_2} < 0.1$	$0.1 \leq S_{CO_2} < 0.2$	$S_{CO_2} \geq 0.2$
4 m	6.1±1.8	4.9±1.5	3.3±0.5
7 m	8.0±1.1	7.2±0.9	6.0±0.4
10 m	10.3±0.7	9.9±0.4	9.4±0.1

[a]Values are given in meters.

CONCLUSIONS

The application of the oscillatory compressibility test permits us to study seismic attenuation and velocity dispersion effects because of wave-induced fluid flow in media similar to the Utsira Sand, containing highly heterogeneous distributions of CO_2 and brine. We can observe that these effects may be very significant, with quality factors below 10 in some cases, mainly for CO_2 saturations near 0.1 and correlation lengths above 0.1 m. This physical process may produce significant velocity dispersion; thus it may play important roles in the velocity pushdown effects. Seismic data from these environments are expected to carry information on wave-induced fluid flow effects; thus, further data analysis may permit derivations of useful characteristics about the mesoscopic-scale properties of the fluid distributions, a subject that will be investigated in future works.

The AVA seismic response of a thin bed containing patchy brine-CO_2 distributions such as those found at the Utsira Sand is very similar to that of an elastic thin bed with the same shear velocity and bulk density, but with a compressional velocity equal to that of the patchy-saturated Utsira Sand averaged in the effective data bandwidth. This result is explained by the fact that although the mesoscopic loss is very important in these media, energy losses within the thin bed are not significant because the layer is very thin as compared to the predominant seismic wavelengths. In addition, the differences because of velocity dispersion effects are minimized when using a mean compressional velocity. In the case of multilayer models, the cumulative effects certainly would lead to significant attenuation. However, in this work we assume that the seismic response of the target thin layer does not interfere with those of other layers, and transmission and absorption losses associated with the overburden are included in the source spectrum.

These facts permit us to make use of a prestack spectral inversion algorithm to estimate representative compressional velocities and thicknesses of CO_2-bearing thin beds, information which could be used to provide a broad insight into CO_2 saturations and volumes. In this sense, results using realistic simulated prestack seismic data show that isolated CO_2-bearing thin beds with properties similar to those of the Utsira Sand could be characterized in terms of their thicknesses and compressional velocities, which allows us to derive some broad but useful information about CO_2 saturations. In this context we show that relatively low velocities are indicative of CO_2 saturations above 0.2–0.4, while relatively high velocities are indicative of low saturations. However, the fact that the correlation length is not known limits the possibility of assessing more accurate saturation estimates, a limitation that becomes more severe for very thin beds.

It is important to remark that this analysis is valid for patchy models with correlation lengths in the range 0.01 m to 0.2 m. As expected, the smaller the correlation length the smaller the uncertainty of the estimates, for inverted velocity and thickness. If the correlation length (or mean size of the CO_2 patches) were known, the information contained in the inverted velocity would allow us to derive more accurate CO_2 saturation estimates from seismic data. Unfortunately this information is not available,

and only rough but very useful CO_2 saturation estimates can be obtained using the proposed method.

Another limitation is that it is not possible to discriminate among saturations above 0.2, an issue that is naturally expected because the compressional velocity at the Utsira Sand does not show any significant change for these saturation levels. In spite of this, we believe that the inverted velocity represents, from a practical point of view, an important petrophysical attribute that can be used as an indicator to characterize CO_2-bearing thin beds. Furthermore, the proposed procedure allows us to obtain reasonable thickness estimates for subtuning CO_2-bearing layers of a few meters. This kind of information is crucial to performing a proper monitoring of the injection process at sites such as the Sleipner field.

ACKNOWLEDGMENTS

The results have been partially obtained in the CO2ReMoVe project, which envisages the development of technologies and procedures for monitoring and verifying geological CO_2 storage. The financial support of the European Commission and the industrial consortium involved is greatly appreciated. We thank Agencia Nacional de Promoción Científica y Tecnológica, Argentina (PICT 03-13376) and Consejo Nacional de Investigaciones Científicas y Técnicas (CONICET, PIP 04-5126) for continuing support. This work was supported in part by a grant from the Swiss National Science Foundation. We are grateful to three anonymous reviewers for their useful comments and suggestions that helped to improve this work.

REFERENCES

Arts, R. J., R. A. Chadwick, O. Eiken, S. Thibeau, and S. Nooner, 2008, Ten years' experience of monitoring CO_2 injection in the Utsira Sand at Sleipner, offshore Norway: First Break **26**, 65–72.

Arts, R., O. Eiken, A. Chadwick, P. Zweigel, L. van der Meer, and B. Zinszner, 2004, Monitoring of CO_2 injected at Sleipner using time-lapse seismic data: Energy **29**, 1383–1392.

Carcione, J. M., and S. Picotti, 2006, P-wave seismic attenuation by slow-wave diffusion: Effects of inhomogeneous rock properties: Geophysics, **71**, no.**3**, O1–O8, doi:10.1190/1.2194512.

Carcione, J. M., S. Picotti, D. Gei, and G. Rossi, 2006, Physics and seismic modeling for monitoring CO_2 storage: Pure and Applied Geophysics **163**, 175–207.

Chadwick, R. A., G. Williams, N. Delepine, V. Clochard, K. Labat, S. Sturton, M.-L. Buddensiek, M. Dillen, M. Nickel, A. L. Lima, R. Arts, F. Neele, and G. Rossi, 2010, Quantitative analysis of time-lapse seismic monitoring data at the Sleipner CO_2 storage operation: The Leading Edge **29**, 170–177.

Chadwick, R. A., R. Arts, and O. Eiken, 2005, 4D seismic quantification of a growing CO_2 plume at the Sleipner, North Sea: Petroleum Geology: North-west Europe and global perspectives: Proceedings of the 6th Petroleum Geology Conference, Geological Society, 1385–1399.

Chung, H.-M., and D. C. Lawton, 1995, Frequency characteristics of seismic reflections from thin beds: Canadian Journal of Exploration Geophysicists, **31**, 32–37.

Clochard, V., N. Delépine, K. Labat, and P. Ricarte, 2009, Post-stack versus pre-stack stratigraphic inversion for CO_2 monitoring purposes: A case study for the saline aquifer of the Sleipner field: 79th Annual International Meeting, SEG, Expanded Abstracts, 2417–2421.

Delépine, N., V. Clochard, K. Labat, P. Ricarte, and C. Le Bras, 2009, Stratigraphic inversion for CO_2 monitoring purposes—A case study for the saline aquifer of Sleipner Field: 71st Conference and Exhibition, EAGE, Extended Abstracts.

Duan, Z., N. Møller, and J. H. Weare, 1992, An equation of state for the CH_4-CO_2-H_2O system: I. Pure systems from 0 to 1000°C and 0 to 8000 bar: *Geochimica et Cosmochimica Acta* **56**, 2605–2617.

Frankel, A., and R. W. Clayton, 1986, Finite difference simulations of seismic scattering: Implications for the propagation of short-period seismic waves in the crust and models of crustal heterogeneity: Journal of Geophysical Research, **91**, 6465–6489, doi:10.1029/JB091iB06p06465.

Ghaderi, A., and M. Landrø, 2009, Estimation of thickness and velocity changes of injected carbon dioxide layers from prestack time-lapse seismic data: Geophysics, **74**, no.**2**, O17–O28, doi:10.1190/1.3054659

Helle, H. B., N. H. Pham, and J. M. Carcione, 2003, Velocity and attenuation in partially saturated rocks: Poroelastic numerical experiments: Geophysical Prospecting, **51**, 551–566, doi:10.1046/j. 1365-2478.2003.00393.x.

Johnson, D. L., 2001, Theory of frequency dependent acoustics in patchy-saturated porous media: Journal of the Acoustical Society of America, **110**, 682–694, doi:10.1121/1.1381021.

Lumley, D., 4D seismic monitoring of CO_2 sequestration: The Leading Edge **29**, 150–155 (2010).

Norris, A. N., 1993, Low-frequency dispersion and attenuation in partially saturated rocks: Journal of the Acoustical Society of America, **94**, 359–370, doi:10.1121/1.407101.

Pride, S. R., and J. G. Berryman, 2003, Linear dynamics of double-porosity dual-permeability materials. I. Governing equations and acoustic attenuation: Physical Review E: statistical, nonlinear, and soft matter physics, **68**, 036603, doi:10.1103/PhysRevE. 68.036603.

Pride, S. R., J. G. Berryman, and J. M. Harris, 2004, Seismic attenuation due to wave-induced flow: Journal of Geophysical Research, **109**, B01201, doi:10.1029/2003JB002639.

Rubino, J. G., C. L. Ravazzoli, and J. E. Santos, 2009, Equivalent viscoelastic solids for heterogeneous fluid-saturated porous rocks: Geophysics, **74**, no. 1, N1–N13, doi: 10.1190/1.3008544.

Rubino, J. G., J. E. Santos, S. Picotti, and J. M. Carcione, 2007, Simulation of upscaling effects due to wave-induced fluid flow in Biot media using the finite-element method: Journal of Applied Geophysics, **62**, 193–203, doi:10.1016/j.jappgeo. 2006.11.003.

Rubino, J. G., and D. R. Velis, 2009, Thin-bed prestack spectral inversion: Geophysics, **74**, no. 4, R49–R57, doi:10.1190/1.3148002.

White, J. E., 1975, Computed seismic speeds and attenuation in rocks with partial gas saturation: Geophysics, **40**, 224–232, doi:10.1190/1.1440520.

White, J. E., N. G. Mikhaylova, and F. M. Lyakhovitskiy, Low-frequency seismic waves in fluid saturated layered rocks: Izvestija, Academy of Sciences, USSR: Physics of the Solid Earth **11**, 654–659 (1975).